

UvA-DARE (Digital Academic Repository)

A platinum(II) metallonitrene with a triplet ground state

Sun, J.; Abbeneth, J.; Verplancke, H.; Diefenbach, M.; de Bruin, B.; Hunger, D.; Würtele, C.; van Slageren, J.; Holthausen, M.C.; Schneider, S.

DOI

[10.1038/s41557-020-0522-4](https://doi.org/10.1038/s41557-020-0522-4)

Publication date

2020

Document Version

Final published version

Published in

Nature Chemistry

License

Article 25fa Dutch Copyright Act

[Link to publication](#)

Citation for published version (APA):

Sun, J., Abbeneth, J., Verplancke, H., Diefenbach, M., de Bruin, B., Hunger, D., Würtele, C., van Slageren, J., Holthausen, M. C., & Schneider, S. (2020). A platinum(II) metallonitrene with a triplet ground state. *Nature Chemistry*, 12(11), 1054-1059. <https://doi.org/10.1038/s41557-020-0522-4>

General rights

It is not permitted to download or to forward/distribute the text or part of it without the consent of the author(s) and/or copyright holder(s), other than for strictly personal, individual use, unless the work is under an open content license (like Creative Commons).

Disclaimer/Complaints regulations

If you believe that digital publication of certain material infringes any of your rights or (privacy) interests, please let the Library know, stating your reasons. In case of a legitimate complaint, the Library will make the material inaccessible and/or remove it from the website. Please Ask the Library: <https://uba.uva.nl/en/contact>, or a letter to: Library of the University of Amsterdam, Secretariat, Singel 425, 1012 WP Amsterdam, The Netherlands. You will be contacted as soon as possible.

UvA-DARE is a service provided by the library of the University of Amsterdam (<https://dare.uva.nl>)



A platinum(II) metallonitrene with a triplet ground state

Jian Sun¹, Josh Abbeneth¹, Hendrik Verplancke², Martin Diefenbach²,
Bas de Bruin³, David Hunger⁴, Christian Würtele¹, Joris van Slageren⁴,
Max C. Holthausen²✉ and Sven Schneider¹✉

Metallonitrenes (M–N) are complexes with a subvalent atomic nitrogen ligand that have been proposed as key reactive intermediates in nitrogen atom transfer reactions. However, in contrast to the common classes of nitride complexes (M≡N) and organic nitrenes (R–N), structurally and spectroscopically well defined ‘authentic’ metallonitrenes with a monovalent atomic nitrogen ligand remain elusive. Here we report that the photolysis of a platinum(II) pincer azide complex enabled the crystallographic, spectroscopic, magnetic and computational characterization of a metallonitrene that is best described as a singly bonded atomic nitrogen diradical ligand bound to platinum(II). The photoproduct exhibits selective C–H, B–H and B–C nitrogen atom insertion reactivity. Despite the subvalent metallonitrene character, mechanistic analysis for aldehyde C–H amidation shows nucleophilic reactivity of the N-diradical ligand. Ambiphilic reactivity of the metallonitrene is indicated by reactions with CO and PMe₃ to form isocyanate and phosphoraneiminato platinum(II) complexes, respectively.

Rational synthetic method development is driven by the ability to relate reactivity to the electronic structures of key transient intermediates. For example, organic nitrenes (R–N) are generally highly reactive monovalent nitrogen species and detailed spectroscopic studies have enabled the assignment of their diverse reaction pathways, such as C–H insertion or N–N coupling, to the accessibility of triplet versus (open shell) singlet spin states^{1,2}. In comparison, the well-established class of nitrido complexes (L_nMN) commonly features trivalent nitrogen with significant covalent components of M–N σ - and π -bonding (Fig. 1a)³. Increased radical and electrophilic nitrogen character can be formally represented by divalent nitridyl all the way to monovalent metallonitrene contributions⁴. Formal nitrido complexes with predominant subvalent metallonitrene (L_nM–N) character, which can be regarded as metal analogues of organic nitrenes, have been proposed as key intermediates in stoichiometric intramolecular^{5–9} and intermolecular^{10–15} nitrogen atom transfer reactions. However, in contrast to organic nitrenes¹⁶, authentic metallonitrenes with a monovalent atomic nitrogen ligand remain elusive, which impedes the development of new nitrogen transfer reactions based on electronic structure/reactivity relationships.

The emergence of C–H amination and amidation via nitrene transfer as a powerful synthetic tool was fuelled by the development of group 9–11 transition metal catalysts that facilitate selective insertion of coordinated nitrene fragments (Fig. 1b)^{17–19}. Late transition metals are also instrumental as anode materials in electrocatalytic amine oxidation for synthetic and fuel cell applications^{20–22}. The dominance of late transition metals in redox transformations of nitrogenous species stimulated fundamental interest in M–N(R) bonding³. C–H insertion by L_nM–NR species has been associated with electrophilic subvalent nitrene (³NR)²³ or imidyl (²NR[•])^{24–26} character that arises from low lying *d* orbitals of late transition met-

als. This strongly reduces the imido (¹NR²⁻) contribution^{27,28}. Similar considerations might apply for metallonitrene (L_nM–N) or nitridyl (L_nM=N[•]) versus nitrido (L_nM≡N) species (Fig. 1a). However, intermolecular C–H activation has not been reported for the few known late transition metal nitrido or nitridyl complexes^{29–31}. The exploitation of nitrogen atom insertion reactivity (Fig. 1b) is still in its infancy; as of yet, catalytic protocols are not known and systematic advances suffer from the lack of well-defined metallonitrene platforms.

In this contribution, a formal nitrido complex beyond group 9 is reported. Crystallographic, spectroscopic, magnetic and computational characterization shows a triplet electronic ground state with a predominantly single-bonded metallonitrene (L_nPt^{II}–N) and nitrogen-centred diradical character. Facile N-atom insertion into C–H, B–H and B–C bonds is demonstrated. In contrast to the generally observed electrophilicity of nitrenes^{17,19}, mechanistic analysis for aldehyde amidation shows evidence of nucleophilic reactivity of the subvalent diradical metallonitrene.

Results and discussion

Generation and characterization of metallonitrene [Pt(N)N(CHCHP^tBu₂)₂]. The platinum(II) azide complex [Pt(N₃)(PNP)] (1, PNP = N(CHCHP^tBu₂)₂) is obtained from the respective chloride precursor in a three-step synthesis (Supplementary Section 1.2). Photolysis in the solid state or in solution with a Xe arc lamp ($\lambda_{\text{exc}} > 305$ nm) or a violet light-emitting diode (LED) ($\lambda = 390$ nm) results in gradual bleaching of the azide band in the infrared (IR) spectrum at 2052 cm⁻¹. A brown product is obtained with several electronic absorption bands in the 360–600 nm range. At temperatures above approximately 223 K (toluene) or 253 K (THF), the spectroscopic signature of the photoproduct vanishes, indicating thermal instability.

¹Universität Göttingen, Institut für Anorganische Chemie, Göttingen, Germany. ²Institut für Anorganische und Analytische Chemie, Goethe-Universität, Frankfurt am Main, Germany. ³van 't Hoff Institute for Molecular Sciences (HIMS), University of Amsterdam, Amsterdam, The Netherlands. ⁴Institut für Physikalische Chemie, Universität Stuttgart, Stuttgart, Germany. ✉e-mail: max.holthausen@chemie.uni-frankfurt.de; sven.schneider@chemie.uni-goettingen.de

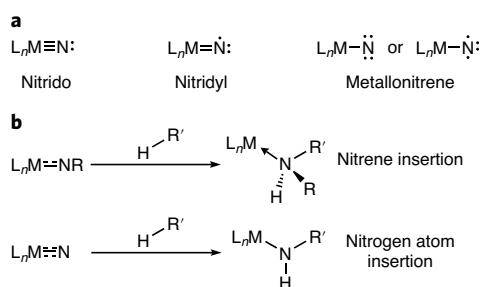


Fig. 1 | Lewis structures and C-H nitrogen insertion reactivity of coordinated nitrogen ligands. **a**, Lewis representations for nitrido, nitridyl and metallonitrene character. **b**, C-H functionalization via metal-mediated nitrene insertion (top) versus nitrogen atom insertion (bottom) (L = ligands, R and R' = organic substituents).

Structural characterization of the photoproduct was therefore carried out by photocrystallography^{32–34}. Photolysis of a single crystal of **1** at 100 K with a violet LED ($\lambda_{exc} = 390$ nm) gave rise to conversion over several hours. Crystallographic monitoring within space group $P\bar{1}$ showed the depletion of electron density in the region of the azide N_β and N_γ atoms. This was accompanied by a rise of electron density in the void defined by the ^tBu substituents of the pincer ligand. The crystallographic data were refined with a partial occupation model of azide **1** and the photoproducts, that is [Pt(N(PNP))] (**2**; Fig. 2a) and free N_2 trapped in the crystal lattice at a distance of over 3 Å from the Pt–N moiety, confirming full scission of the azide N_α – N_β bond. Satisfactory crystallographic data were obtained up to a photoconversion of 76%, offering reliable metrical parameters of the molecular structure of **2**.

In comparison with parent **1**, the structure of **2** exhibits only small deviations within the Pt(PNP) framework. The approximately linear N–Pt–N axis is maintained (N–Pt–N angle: 176.0(4)°) and slight

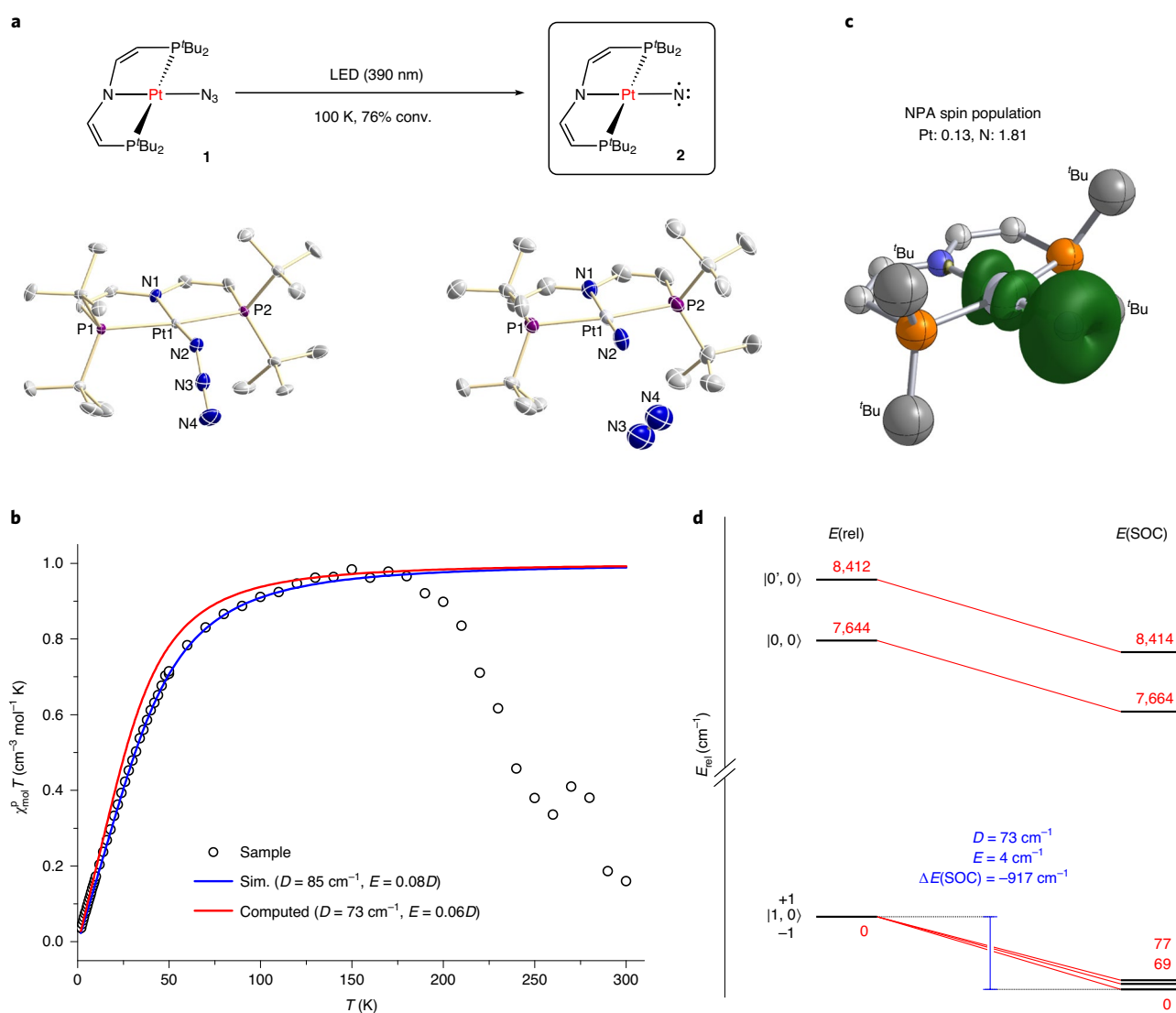


Fig. 2 | Synthesis, crystallographic and magnetic characterization of platinum(II) metallonitrene **2.** **a**, Molecular structure of **2** obtained by in situ photolysis of a single-crystal of **1** (H atoms omitted for clarity). Selected bond lengths (Å) and angles (°) of **1**: Pt1–N1 2.011(5), Pt1–N2 2.031(5), Pt1–P1 2.3171(13), Pt1–P2 2.3125(13), P2–Pt1–P1 165.77(5), N1–Pt1–N2 174.4(2); and of **2**: Pt1–N1 2.068(7), Pt1–N2 1.874(11), Pt1–P1 2.3050(19), Pt1–P2 2.303(2), P2–Pt1–P1 164.88(8), N1–Pt1–N2 176.0(4). **b**, $\chi_{mol}T$ versus T data (circles) of in situ ($\lambda_{exc} = 390$ nm) formed **2** obtained by superconducting quantum interference device magnetometry with simulated (blue line) and ab initio computed (red line) values. **c**, Computed spin density distribution and NPA spin population (isosurface at 0.0075 a_0^{-3} ; PBE0/def2-TZVPP results). **d**, State correlation diagram from CASSCF/NEVPT2 calculations for the triplet ground state of **2** with scalar relativistic energies, $E(rel)$, and energies including spin-orbit coupling, $E(SOC)$.

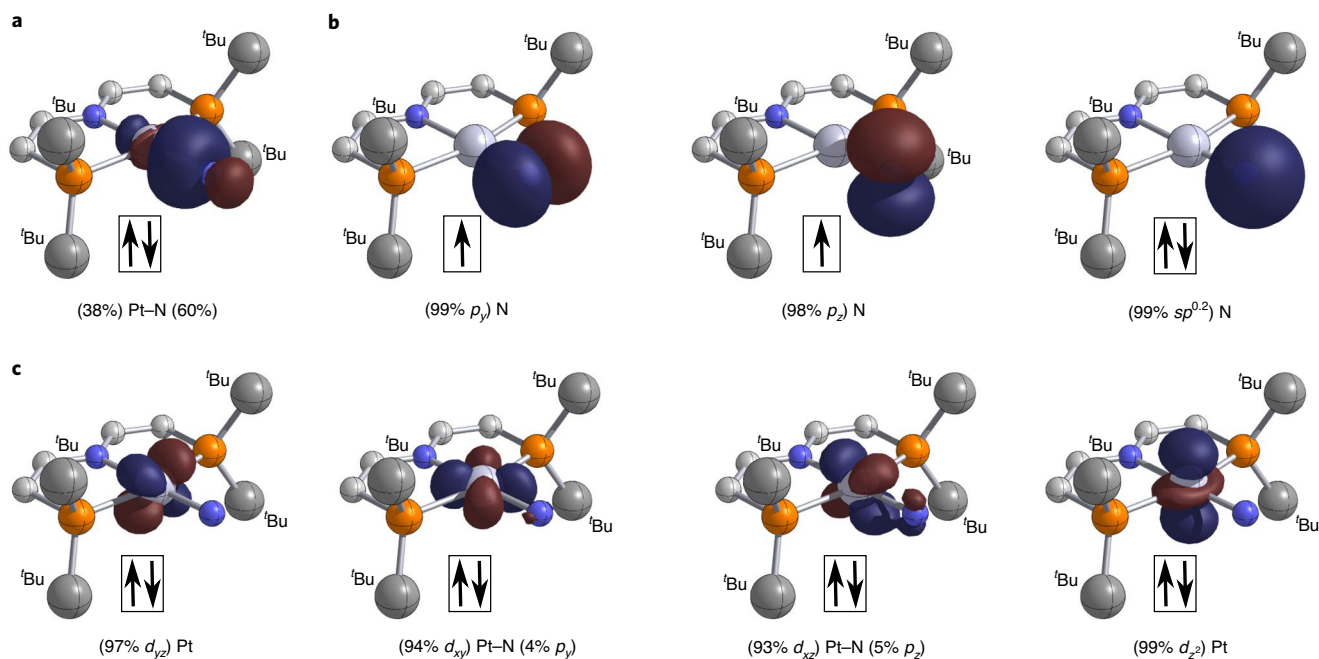


Fig. 3 | Characteristic NLMOs resulting from an NBO analysis support the platinum(II) metallonitrene description of complex **2.** Isosurfaces at $\pm 0.05 a_0^{-3/2}$, results for doubly occupied orbitals were obtained by averaging over the α and β spin orbitals. **a**, Pt–N σ bond. **b**, Singly occupied p_x and p_z orbitals and s -type lone pair localized at N. **c**, Pt-centred, doubly occupied d orbitals.

elongation of the Pt–N_{PNP} bond ($\Delta d = 0.06 \text{ \AA}$) indicates increased *trans* influence. In turn, the distance to the atomic nitrogen ligand ($d_{\text{Pt–N}} = 1.874(11) \text{ \AA}$) is at the lower end of experimentally observed Pt–N bond lengths³⁵ and significantly shortened with respect to **1** (Pt–N₃ distance: 2.031(5) \AA) or an independently prepared parent amide complex (Pt(NH₂)(PNP)) (**3**; Pt–NH₂ distance: 2.030(3) \AA). A similar bond length (1.81 \AA) was computed for the Pt=O core in Milstein's platinum oxo complex^{36,37}. However, in that case the oxo ligand was predicted to be strongly bent out of the Pt(PCN) plane (C–Pt–O angle: 138.2°). Based on Pyykkö's covalent radii, 1.94, 1.72 and 1.64 \AA are expected for Pt–N single, double and triple bond lengths, respectively³⁸.

The observation of three paramagnetically broadened and shifted ¹H NMR signals is in agreement with an open shell C_{2v} symmetric ground state, similar to isoelectronic ³[Ir(E)(PNP)] (E = NtBu, O)^{39,40}. Linear dependence of $\delta(^1\text{H})$ on T^{-1} indicates population of a single electronic state in the range 193–253 K. Superconducting quantum interference device magnetometry data were obtained after in situ photolysis of solid azide **1** at 10 K ($\lambda_{\text{exc}} = 390 \text{ nm}$) leading to a constant rise of the d.c. magnetic moment over time. Below 50 K, the molar paramagnetic susceptibility temperature product ($\chi_{\text{m}}T$) of the photoproduct increases approximately linearly with temperature and assumes an almost constant value between 50 and 170 K (Fig. 2b). Beyond that, the magnetic moment rapidly drops, which we attribute to thermal instability of the photoproduct. The magnetic data below 170 K were nicely reproduced with a zero-field splitting (ZFS) spin-Hamiltonian for a triplet ($S = 1$) state with an isotropic g factor ($g = 2$) upon estimating the photochemical conversion by normalization to the expectation value at high temperatures. The obtained axial (D) and rhombic (E) ZFS parameters ($D = 85 \text{ cm}^{-1}$, $E = 0.08D$) are in excellent agreement with the values predicted by multi-reference NEVPT2 spin-orbit computations ($D = 73 \text{ cm}^{-1}$, $E = 0.06D$; Fig. 2b) and in line with the absence of an X-band EPR signal for **2** (in both perpendicular and parallel mode). However, the microstate splitting is considerably smaller compared with the isoelectronic complexes [Ir(NtBu)

(PNP)] ($D = 466 \text{ cm}^{-1}$) and [Ir(O)(PNP)] ($D = 647 \text{ cm}^{-1}$)^{39,40}, indicating decreased effective spin–orbit coupling (ζ_{eff}). As an explanation, ligand-field considerations suggest increased ligand radical character for **2**⁴¹. This is fully supported by the computational analysis, which shows predominantly N-centred biradical character (Fig. 2c).

Quantum-chemical modelling of complex **2** gave square-planar metal coordination for density functional theory (DFT) optimized geometries of both the triplet and singlet states. While the experimental structural parameters are nicely reproduced by the triplet state (for example, $d_{\text{Pt–N}} = 1.89 \text{ \AA}$), the Pt–N bond length is significantly shorter for the singlet species ($d_{\text{Pt–N}} = 1.79 \text{ \AA}$). Explicitly correlated ONIOM coupled-cluster computations (Supplementary Section 4.1) confirmed that the triplet state is strongly stabilized with respect to the lowest singlet by $\Delta E_{\text{S,T}} = 15 \text{ kcal mol}^{-1}$. Spin-orbit coupling effects have no significant influence on the spin-state energetics according to CASSCF/NEVPT2 calculations (Fig. 2d). The composition of natural localized molecular orbitals (NLMOs) evolving from a natural bond orbital (NBO) analysis of the DFT ground-state wave function supports the notion of a {Pt^{II}–N} metallonitrene (natural population analysis charges: $q_{\text{Pt}} = +0.38$, $q_{\text{N(nitrene)}} = -0.52$). The NBO results show a covalent Pt–N σ bond polarized towards nitrogen (Fig. 3a), an s -type lone pair and two singly occupied p -type NLMOs on the nitrene N atom (Fig. 3b) as well as four essentially nonbonding Pt d orbitals (Fig. 3c) that share only insignificant N contributions (Pt–N Wiberg bond order: 0.94). This picture closely resembles an organic nitrene (N–R)^{42,43} with moderately spaced frontier orbitals, resulting in a triplet ground state and a first excited closed-shell singlet state, followed by an open-shell singlet, like methoxy nitrene N–OCH₃¹. Multireference computations fully support this picture and suggest a predominantly (92%) triplet ground-state metallonitrene Pt^{II}(³N) character. Imidyl, Pt^{III}(²N[–]), or related alternative configurations contribute individually by less than 1% to the ground-state wave function (Supplementary Table 38)²³. Our results show **2** as a unique metallonitrene with predominantly single covalent Pt–N bond character without significant π bonding, contrasting with typical nitrido complexes²⁹.

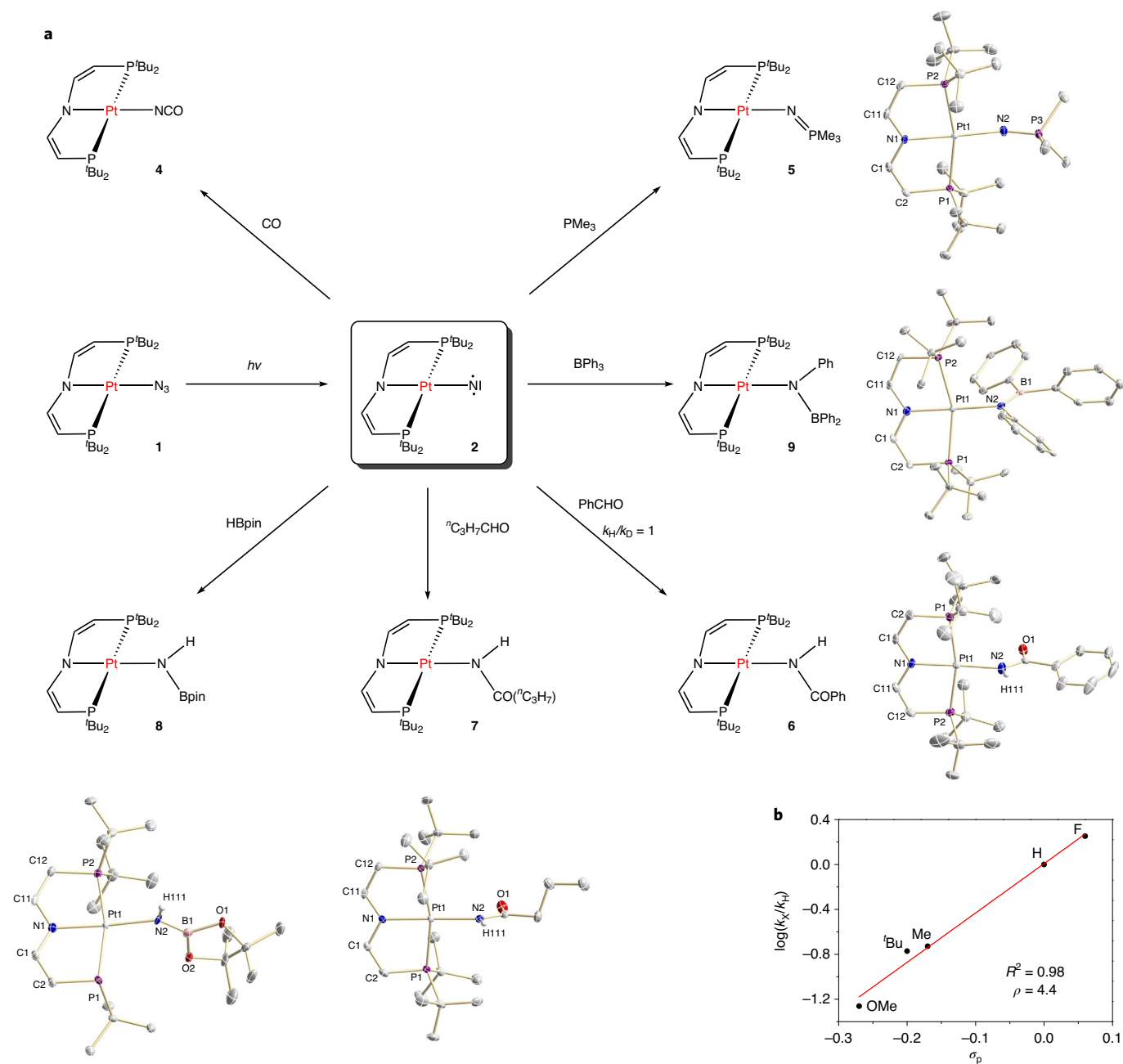


Fig. 4 | Nitrogen centred reactivity of metallonitrene 2. **a**, Ambiphilic reactivity patterns of the metallonitrene with CO, PMe_3 and towards C–H, B–H and B–C insertion reactions (the kinetic isotope effect $k_{\text{H}}/k_{\text{D}}$ was derived from a competition experiment with HC(O)Ph and DC(O)Ph). **b**, The Hammett plot for C–H nitrogen atom insertion with *para*-substituted benzaldehydes, indicating nucleophilic reactivity of the metallonitrene ($k_{\text{X}}/k_{\text{H}}$ = relative rate constants for *para*-X substituted benzaldehydes versus benzaldehyde obtained by competition experiments; σ_{p} = Hammett substituent constant, ρ = reaction constant).

Reactivity of metallonitrene ((Pt(N)(PNP)) (2). The reactivity of metallonitrene 2 was examined by in situ photolysis of 1 ($\lambda_{\text{exc}} > 305 \text{ nm}$). In the presence of CO (1 atm), the platinum(II) isocyanate complex [Pt(NCO)(PNP)] (4) was obtained with high selectivity and could be isolated in around 60% yield (Fig. 4a). The reaction with PMe_3 gave phosphoraneiminato complex [Pt(NPMe₃)(PNP)] (5) in around 75% spectroscopic yield, which could be characterized crystallographically (Fig. 4a), indicating facile crossing onto the singlet surface upon nucleophilic attack¹⁶. Nitrogen atom transfer was further examined with selected electrophiles. Insertion into C–H, B–H and B–C bonds was obtained in the presence of 1.1–1.5 equiv. benzaldehyde, 1-butanal, 4,4,5,5-tetramethyl-1,3,2-dioxaborolane

(HBpin) and triphenylborane, respectively, giving the platinum(II) amido complexes 6–9 in over 80% (6–8) and 39% (9) isolated yields, respectively (Fig. 4a). Photolysis of 1 in toluene-*d*₈ at -70°C and subsequent addition of benzaldehyde also gave the amide product 6 as the main product after warming to room temperature in the dark, supporting thermal amide formation from the metallonitrene intermediate.

Aldehyde C–H amidation was examined in more detail to distinguish between conceivable pathways. Photolysis of 1 in the presence of PhC(O)H/PhC(O)D (5 equiv. each) indicated the absence of a kinetic isotope effect. Competition experiments with a series of *para*-substituted benzaldehydes gave rise to a Hammett plot with

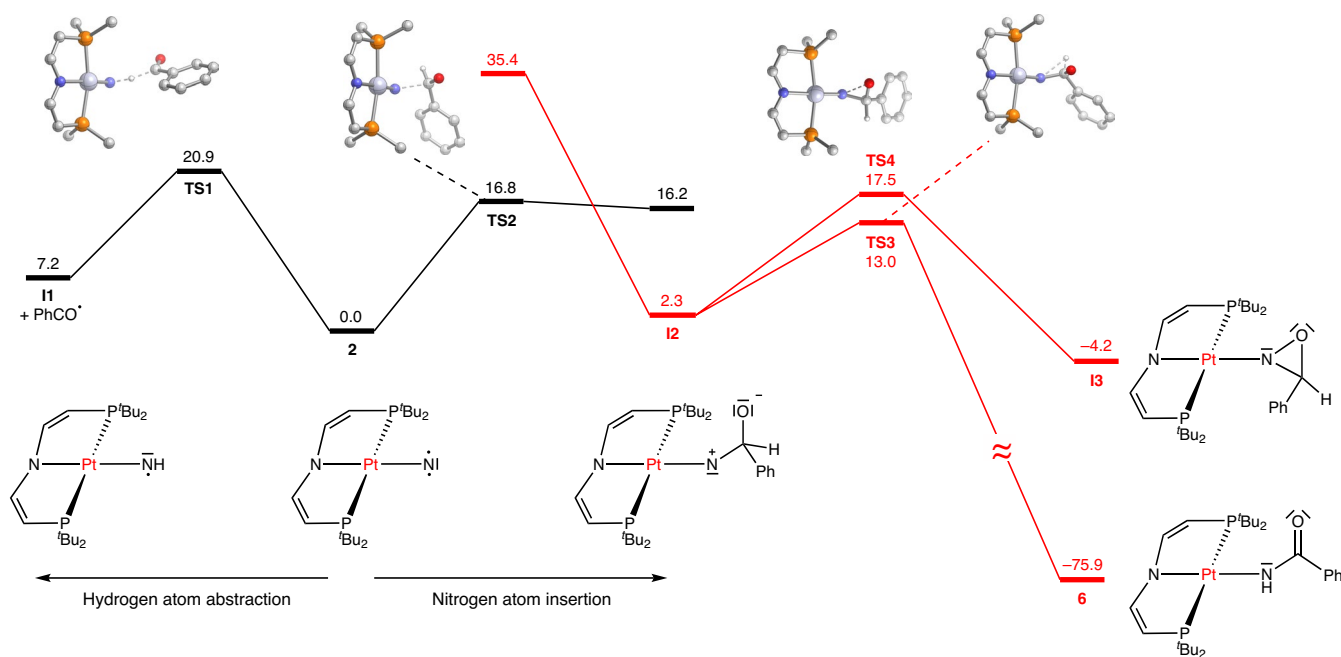


Fig. 5 | Computational examination of the reaction of metallonitrene 2 with benzaldehyde. Calculated pathways for the reaction of **2** (full model) with PhCHO (ONIOM(CCSD(T*)-F12:PBE0-D) support nucleophilic attack of the triplet metallonitrene at the carbonyl group as the preferred pathway (triplet surface in black and singlet surface in red; ΔG in kcal mol⁻¹; only tertiary carbon atoms of ^tBu groups shown for ball and stick figures).

a steep positive slope (reaction constant $\rho = +4.4$, Fig. 4b)⁴⁴. These observations are consistent with rate-determining nucleophilic attack of the metallonitrene at the carbonyl group. Importantly, the reactivity of **2** does obviously not encompass radical rebound pathways via hydrogen atom abstraction (HAA) here, despite the diradical nature of the nitrene and comparatively small aldehyde C–H bond dissociation energies⁴⁵.

Further mechanistic rationalization of aldehyde amidation is provided by computational investigations. Explicitly correlated ONIOM coupled-cluster calculations were used to compare nucleophilic versus radical reactivity of **2** (Fig. 5). The radical HAA from benzaldehyde is connected with a free energy barrier of 20.9 kcal mol⁻¹ (TS1). Nucleophilic attack of triplet species **2** at the benzaldehyde via TS2 ($\Delta G^\ddagger = 16.8$ kcal mol⁻¹) is clearly favoured over HAA and leads to tetrahedral intermediate **I2**. Similar to **2**, triplet TS2 lacks significant contributions from other configurations, excluding imidyl- or nitride-driven reactivity. The ONIOM coupled-cluster results show a singlet ground state for **I2**, in full accordance with multi-reference NEVPT2 results. By contrast, DFT erroneously favours a triplet ground state (Supplementary Table 40) as similarly reported for related copper nitrene complexes^{46,47}. The singlet and triplet potential energy surfaces cross beyond transition state TS2 along the reaction coordinate leading to **I2**. The estimated crossing point is approximately isoenergetic with TS2, which excludes any significant lowering of the activation barrier in the sense of a two-state reactivity scenario^{48,49}. Two pathways branch off from **I2**, that is, formation of amide **6** or alternatively ring closure to form oxaziridine **I3**, as typically observed for singlet aryl nitrenes⁵⁰. However, oxaziridine formation is reversible under the reaction conditions and is both kinetically and thermodynamically disfavoured. The experimentally observed product **6** is formed from **I2** with a modest barrier of 10.7 kcal mol⁻¹ via TS3 in a highly exergonic step ($\Delta_r G = -75.9$ kcal mol⁻¹). Thus, nucleophilic attack of the triplet metallonitrene at the carbonyl group represents the overall rate-determining step and neither the transition to the singlet potential energy surface nor the subsequent

hydrogen shift are kinetically significant, in full agreement with the Hammett analysis and the absence of a hydrogen/deuterium kinetic isotope effect.

Conclusions

In summary, the metallonitrene **2** was synthesized upon photolysis of azide complex **1**. Complex **2** exhibits a triplet electronic ground state with unexpectedly low microstate splitting as a result of dominant ligand radical character. Our detailed bonding analysis supports the picture of a {(PNP)Pt^{III}} fragment with a single covalent σ bond to an atomic nitrogen diradical ligand in distinct contrast to the common triply bonded nitrido description. Complex **2** exhibits versatile and selective ambiphilic intermolecular reactivity exemplified, for example, by the formation of phosphoraneiminato product **5** and reaction with aldehydes and boranes that leads to facile nitrogen atom insertion into C–H, B–H and B–C bonds. Experimental and computational mechanistic data for aldehyde amidation favour rate-determining nucleophilic attack of the nitrogen atom over initial (proton coupled) electron transfer pathways, such as a HAA/radical rebound mechanism, which is surprising given its subvalent diradical nature. This work provides a detailed view of the electronic structure of metallonitrenes and emphasizes the fact that, in contrast to intuition, neither the subvalent character nor the open-shell nature of the ground state are reliable predictors for nitrogen atom transfer reactivity⁵¹.

Online content

Any methods, additional references, Nature Research reporting summaries, source data, extended data, supplementary information, acknowledgements, peer review information; details of author contributions and competing interests; and statements of data and code availability are available at <https://doi.org/10.1038/s41557-020-0522-4>.

Received: 6 January 2020; Accepted: 8 July 2020;
Published online: 24 August 2020

References

1. Falvey, D. E. & Gudmundsdottir, A. D. *Nitrenes and Nitrenium Ions* (John Wiley & Sons, 2013).
2. Wentrup, C. Carbenes and nitrenes: recent developments in fundamental chemistry. *Angew. Chem. Int. Ed.* **57**, 11508–11521 (2018).
3. Berry, J. F. Terminal nitrido and imido complexes of the late transition metals. *Comments Inorg. Chem.* **30**, 28–66 (2009).
4. Suarez, A. I. O., Lyaskovskyy, V., Reek, J. N. H., van der Vlugt, J. I. & Bruin, B. Complexes with nitrogen-centered radical ligands: classification, spectroscopic features, reactivity, and catalytic applications. *Angew. Chem. Int. Ed.* **52**, 12510–12529 (2013).
5. Hojilla Atienza, C. C., Bowman, A. C., Lobkovsky, E. & Chirik, P. J. Photolysis and thermolysis of Bis(imino)pyridine cobalt azides: C–H activation from putative cobalt nitrido complexes. *J. Am. Chem. Soc.* **132**, 16343–16345 (2010).
6. Thomson, R. K. et al. Uranium azide photolysis results in C–H bond activation and provides evidence for a terminal uranium nitride. *Nat. Chem.* **2**, 723–729 (2010).
7. King, D. M. et al. Isolation and characterization of a uranium(VI)–nitride triple bond. *Nat. Chem.* **5**, 482–488 (2013).
8. Schöffel, J., Šušnjar, N., Nüchel, S., Sieh, D. & Burger, P. 4d vs. 5d – Reactivity and Fate of Terminal Nitrido Complexes of Rhodium and Iridium. *Eur. J. Inorg. Chem.* **2010**, 4911–4915 (2010).
9. Vreeken, V. et al. C–H activation of benzene by a photoactivated Ni^{II}(azide): Formation of a transient nickel nitrido complex. *Angew. Chem. Int. Ed.* **54**, 7055–7059 (2015).
10. Henning, H., Hofbauer, K., Handke, K. & Stich, R. Unusual reaction pathways in the photolysis of diazido(phosphane)nickel(II) complexes: nitrenes as intermediates in the formation of nickel(0) complexes. *Angew. Chem. Int. Ed. Engl.* **36**, 408–410 (1997).
11. Ronconi, L. & Sadler, P. J. Unprecedented carbon–carbon bond formation induced by photoactivation of a platinum(IV)–diazido complex. *Chem. Commun.* 235–237 (2008).
12. Yao, C., Wang, X. & Huang, K.-W. Nitrogen atom transfer mediated by a new PN³P–pincer nickel core via a putative nitrido nickel intermediate. *Chem. Commun.* **54**, 3940–3943 (2018).
13. Ghannam, J. et al. Intramolecular C–H functionalization followed by a $[2\sigma+2\pi]$ addition via an intermediate nickel–nitridyl complex. *Inorg. Chem.* **58**, 7131–7135 (2019).
14. Sun, Z., Hull, O. A. & Cundari, T. R. Computational study of methane C–H activation by diiminopyridine nitride/nitridyl complexes of 3d transition metals and main-group elements. *Inorg. Chem.* **57**, 6807–6815 (2018).
15. Man, W.-L., Lam, W. W. Y., Kwong, H.-K., Yiu, S.-M. & Lau, T.-C. Ligand-accelerated activation of strong C–H bonds of alkanes by a (Salen)ruthenium(VI)–nitrido complex. *Angew. Chem. Int. Ed.* **51**, 9101–9104 (2012).
16. Dielmann, F. et al. A crystalline singlet phosphonitrene: a nitrogen atom–transfer agent. *Science* **337**, 1526–1528 (2012).
17. Kuijpers, P. F., van der Vlugt, J. I., Schneider, S. & de Bruin, B. Nitrene radical intermediates in catalytic synthesis. *Chem. Eur. J.* **23**, 13819–13829 (2017).
18. Davies, H. M. L. & Manning, J. R. Catalytic C–H functionalization by metal carbenoid and nitrenoid insertion. *Nature* **451**, 417–424 (2008).
19. Park, Y., Kim, Y. & Chang, S. Transition metal-catalyzed C–H amination: scope, mechanism, and applications. *Chem. Rev.* **117**, 9247–9301 (2017).
20. Rosca, V., Duca, M., de Groot, M. T. & Koper, M. T. M. Nitrogen cycle electrocatalysis. *Chem. Rev.* **109**, 2209–2244 (2009).
21. Zhao, Y. et al. An efficient direct ammonia fuel cell for affordable carbon-neutral transportation. *Joule* **3**, 2472–2484 (2019).
22. Siu, T. & Yudin, A. K. Practical olefin aziridination with a broad substrate scope. *J. Am. Chem. Soc.* **124**, 530–531 (2002).
23. Carsch, K. M. et al. Synthesis of a copper-supported triplet nitrene complex pertinent to copper-catalyzed amination. *Science* **365**, 1138–1143 (2019).
24. Iluc, V. M. et al. Synthesis and characterization of three-coordinate Ni(III)–imide complexes. *J. Am. Chem. Soc.* **133**, 13055–13063 (2011).
25. Lyaskovskyy, V. et al. Mechanism of cobalt(II) porphyrin-catalyzed C–H amination with organic azides: radical nature and H-atom abstraction ability of the key cobalt(III)–nitrene intermediates. *J. Am. Chem. Soc.* **133**, 12264–12273 (2011).
26. Goswami, M. et al. Characterization of porphyrin-Co(III)–‘nitrene radical’ species relevant in catalytic nitrenetransfer reactions. *J. Am. Chem. Soc.* **137**, 5468–5479 (2015).
27. Laskowski, C. A., Miller, A. J. M., Hillhouse, G. L. & Cundari, T. R. A. Two-coordinate nickel imido complex that effects C–H amination. *J. Am. Chem. Soc.* **133**, 771–773 (2011).
28. Grünwald, A. et al. An isolable terminal imido complex of palladium and catalytic implications. *Angew. Chem. Int. Ed.* **57**, 16228–16232 (2018).
29. Schöffel, J., Rogachev, A. Y., DeBeer George, S. & Burger, P. Isolation and hydrogenation of a complex with a terminal iridium–nitrido bond. *Angew. Chem. Int. Ed.* **48**, 4734–4738 (2009).
30. Scheibel, M. G. et al. Closed-shell and open-shell square-planar iridium nitrido complexes. *Nat. Chem.* **4**, 552–558 (2012).
31. Zolnhofer, E. M. et al. An intermediate cobalt(IV) nitrido complex and its N-migratory insertion product. *J. Am. Chem. Soc.* **136**, 15072–15078 (2014).
32. Cole, J. M. Single-crystal X-ray diffraction studies of photo-induced molecular species. *Chem. Soc. Rev.* **33**, 501–513 (2004).
33. Das, A., Reibenspies, J. H., Chen, Y.-S. & Powers, D. C. Direct characterization of a reactive lattice-confined Ru₂ nitride by photocrystallography. *J. Am. Chem. Soc.* **139**, 2912–2915 (2017).
34. Das, A., Chen, Y.-S., Reibenspies, J. H. & Powers, D. C. Characterization of a reactive Rh₂ nitrenoid by crystalline matrix isolation. *J. Am. Chem. Soc.* **141**, 16232–16236 (2019).
35. Cook, A. W. et al. Synthesis and characterization of a linear, two-coordinate Pt(II) ketimide complex. *Inorg. Chem.* **58**, 15927–15935 (2019).
36. Poverenov, E. et al. Evidence for a terminal Pt(IV)–oxo complex exhibiting diverse reactivity. *Nature* **455**, 1093–1096 (2008).
37. Efremenko, I., Poverenov, E., Martin, J. M. L. & Milstein, D. DFT Study of the structure and reactivity of the terminal Pt(IV)–oxo complex bearing no electron-withdrawing ligands. *J. Am. Chem. Soc.* **132**, 14886–14900 (2010).
38. Pyykkö, P. Additive covalent radii for single-, double-, and triple-bonded molecules and tetrahedrally bonded crystals: a summary. *J. Phys. Chem. A* **119**, 2326–2337 (2015).
39. Kinauer, M. et al. An iridium(III/IV/V) redox series featuring a terminal imido complex with triplet ground state. *Chem. Sci.* **9**, 4325–4332 (2018).
40. Delony, D. et al. A terminal iridium oxo complex with a triplet ground state. *Angew. Chem. Int. Ed.* **58**, 10971–10974 (2019).
41. Singh, S. K., Eng, J., Atanasov, M. & Neese, F. Covalency and chemical bonding in transition metal complexes: An ab initio based ligand field perspective. *Coord. Chem. Rev.* **344**, 2–25 (2017).
42. Yarkony, D. R., Schaefer, H. F. & Rothenberg, S. X³A₂, a¹E, and b¹A₁ electronic states of methylnitrene. *J. Am. Chem. Soc.* **96**, 5974–5977 (1974).
43. Borden, W. T. et al. The interplay of theory and experiment in the study of phenylnitrene. *Acc. Chem. Res.* **33**, 765–771 (2000).
44. Hansch, C., Leo, A. & Taft, R. W. A survey of Hammett substituent constants and resonance and field parameters. *Chem. Rev.* **91**, 165–195 (1991).
45. Oyeemi, V. B., Keith, J. A. & Carter, E. A. Trends in bond dissociation energies of alcohols and aldehydes computed with multireference averaged coupled-pair functional theory. *J. Phys. Chem. A* **118**, 3039–3050 (2014).
46. Tekarli, S. M., Williams, T. G. & Cundari, T. R. Activation of carbon–hydrogen and hydrogen–hydrogen bonds by copper–nitrenes: a comparison of density functional theory with single- and multireference correlation consistent composite approaches. *J. Chem. Theory Comput.* **5**, 2959–2966 (2009).
47. Cundari, T. R., Dinescu, A. & Kazi, A. B. Bonding and structure of copper nitrenes. *Inorg. Chem.* **47**, 10067–10072 (2008).
48. Schröder, D., Shaik, S. & Schwarz, H. Two-state reactivity as a new concept in organometallic chemistry. *Acc. Chem. Res.* **33**, 139–145 (2000).
49. Harvey, J. N. Spin-forbidden reactions: computational insight into mechanisms and kinetics. *WIREs Comput. Mol. Sci.* **4**, 1–14 (2014).
50. Gritsan, N. P. & Platz, M. S. Kinetics, spectroscopy, and computational chemistry of aryl nitrenes. *Chem. Rev.* **106**, 3844–3867 (2006).
51. Saouma, C. T. & Mayer, J. M. Do spin states and spin density affect hydrogen atom transfer reactivity? *Chem. Sci.* **5**, 21–31 (2014).

Publisher's note Springer Nature remains neutral with regard to jurisdictional claims in published maps and institutional affiliations.

© The Author(s), under exclusive licence to Springer Nature Limited 2020

Methods

Synthesis and characterization of complexes 1 and 3–9. [PtN₃(PNP)] (1). [PtOTf(PNP)] (D) (68 mg, 0.10 mmol, 1.00 equiv.) and NaN₃ (34 mg, 0.52 mmol, 5.31 equiv.) were suspended in THF (2 ml). After stirring for 14 h at room temperature in a brown vial, the colour of the mixture changed from light yellow to almost colourless. After removal of the solvent, extraction with Et₂O (5 × 3 ml) and evaporation of the solvent, a white solid was obtained. Extraction with C₆H₆ (approximately 3 ml), filtration and removal of solvent gave **1** as a white solid (yield 52.7 mg, 90%). Crystals suitable for X-ray diffraction were obtained by slow evaporation of an Et₂O solution: ¹H NMR (300.13 MHz, C₆D₆, 298 K): δ (ppm) 6.53 (A₁₈XX'A'₁₈, N = |³J_{HP} + ⁴J_{HP}| = 38.1 Hz, ³J_{HH} = 5.4 Hz, ³J_{PH} = 78.1 Hz, 2H, NCH), 3.91 (A₁₈XX'A'₁₈, N = |³J_{HP} + ⁴J_{HP}| = 9.3 Hz, ³J_{HH} = 5.2 Hz, ³J_{PH} = 33.6 Hz, 2H, PCH), 1.33 (A₁₈XX'A'₁₈, N = |³J_{HP} + ⁵J_{HP}| = 14.4 Hz, 36H, CMe₃); ¹³C{¹H} NMR (75.48 MHz, C₆D₆, 298 K): δ (ppm) 162.6 (t, ²J_{PC} = 7.4 Hz, ²J_{PC} = 81.8 Hz, NCH), 82.8 (t, ¹J_{PC} = 22.8 Hz, ²J_{PC} = 53.2 Hz, CHP), 36.2 (t, ¹J_{PC} = 13.0 Hz, PCMe₃), 29.1 (t, ²J_{PC} = 3.1 Hz, ²J_{PC} = 12.8 Hz, PCMe₃); ³¹P{¹H} NMR (121.49 MHz, C₆D₆, 298 K): δ (ppm) 66.8 (s, ¹J_{PP} = 2,686.5 Hz); ¹⁹⁵Pt{¹H} NMR (107.14 MHz, toluene-d₈, 298 K): δ (ppm) -3,917.4 (t, ¹J_{PP} = 2,719.7 Hz); IR (ATR): 2,052 (N₃), 1,530 (C=C) cm⁻¹; UV-vis (THF): λ_{max} (ε, M⁻¹ cm⁻¹) = 233 (17,160), 260 (7,760), 312 (19,980) nm; MS (LIFDI): *m/z* (%) 593.2 (100); analysis (calculated, found for C₂₀H₄₀N₄P₂Pt): C (40.47, 40.31%), H (6.79, 6.74%), N (9.44, 9.35%).

[PtNH₂(PNP)] (3). [PtOTf(PNP)] (D) (23.7 mg, 0.034 mmol, 1.00 equiv.) and NaNH₂ (8.8 mg, 0.22 mmol, 6.67 equiv.) were suspended in THF (1 ml). After stirring at room temperature for 2 h and removal of the solvent, the residue was extracted with Et₂O (3 ml). After filtration and removal of Et₂O, the residue was extracted with C₆H₆ (2 ml). After filtration and removal of C₆H₆, **3** was obtained as a white solid (yield 15.0 mg, 78%). Crystals suitable for X-ray diffraction were obtained by crystallization from a saturated solution in Et₂O at -36 °C: ¹H NMR (400.25 MHz, C₆D₆, 298 K): δ (ppm) 7.00 (A₁₈XX'A'₁₈, N = |³J_{HP} + ⁴J_{HP}| = 39.2 Hz, ³J_{HH} = 5.2 Hz, ³J_{PH} = 53.2 Hz, 2H, NCH), 4.08 (A₁₈XX'A'₁₈, N = |³J_{HP} + ⁴J_{HP}| = 8.9 Hz, ³J_{HH} = 5.2 Hz, ³J_{PH} = 33.6 Hz, 2H, PCH), 1.35 (A₁₈XX'A'₁₈, N = |³J_{HP} + ⁵J_{HP}| = 14.0 Hz, 36H, CMe₃), 0.52 (s, 2H, NH₂); ¹³C{¹H} NMR (100.65 MHz, C₆D₆, 298 K): δ (ppm) 161.9 (t, ²J_{PC} = 7.5 Hz, ²J_{PC} = 65.5 Hz, NCH), 82.3 (t, ¹J_{PC} = 23.1 Hz, ²J_{PC} = 35.0 Hz, CHP), 36.0 (t, ¹J_{PC} = 12.8 Hz, ²J_{PC} = 37.1 Hz, PCMe₃), 29.2 (t, ²J_{PC} = 3.1 Hz, ²J_{PC} = 15.7 Hz, PCMe₃); ³¹P{¹H} NMR (162.02 MHz, C₆D₆, 298 K): δ (ppm) 60.6 (s, ¹J_{PP} = 2,839.6 Hz); ¹⁹⁵Pt{¹H} NMR (107.13 MHz, C₆D₆, 298 K): δ (ppm) -3,819.8 (t, ¹J_{PP} = 2,864.7 Hz); IR (ATR): 3,288 (N-H), 1,516 (C=C) cm⁻¹; UV-vis (THF): λ_{max} (ε, M⁻¹ cm⁻¹) = 240 (15,740), 332 (16,718) nm; MS (LIFDI): *m/z* (%) 567.2 (100); analysis (calculated, found for C₂₀H₄₂N₂P₂Pt): C (42.32, 42.49%), H (7.46, 7.45%), N (4.94, 4.84%).

[PtNCO(PNP)] (4). Complex **1** (11.0 mg, 0.019 mmol, 1.00 equiv.) was dissolved in C₆D₆ (0.4 ml). The vessel containing the mixture was degassed by three freeze-pump-thaw cycles and refilled with CO (1 atm). The solution was photolysed (λ_{exc} > 305 nm) at room temperature for 2 h. Removal of the solvent in vacuo and washing of the residue with pentane (2 × 1 ml) gave analytically pure complex **4** (yield 6.5 mg, 59%): ¹H NMR (400.25 MHz, C₆D₆, 298 K): δ (ppm) 6.52 (A₁₈XX'A'₁₈, N = |³J_{HP} + ⁴J_{HP}| = 38.8 Hz, ³J_{HH} = 5.6 Hz, ³J_{PH} = 80.3 Hz, 2H, NCH), 3.89 (A₁₈XX'A'₁₈, N = |³J_{HP} + ⁴J_{HP}| = 9.6 Hz, ³J_{HH} = 5.2 Hz, ³J_{PH} = 32.0 Hz, 2H, PCH), 1.27 (A₁₈XX'A'₁₈, N = |³J_{HP} + ⁵J_{HP}| = 14.4 Hz, 36H, CMe₃); ¹³C{¹H} NMR (100.65 MHz, C₆D₆, 298 K): δ (ppm) 162.8 (t, ²J_{PC} = 7.4 Hz, ²J_{PC} = 83.0 Hz, NCH), 82.7 (t, ¹J_{PC} = 22.6 Hz, CHP), 36.2 (t, ¹J_{PC} = 13.2 Hz, PCMe₃), 29.1 (t, ²J_{PC} = 3.0 Hz, PCMe₃); ³¹P{¹H} NMR (162.02 MHz, C₆D₆, 298 K): δ (ppm) 66.4 (s, ¹J_{PP} = 2,608.5 Hz); IR (ATR): 2,253 (NCO), 1,529 (C=C) cm⁻¹; UV-Vis (THF): λ_{max} (ε, M⁻¹ cm⁻¹) = 237 (12,110), 248 (11,600), 319 (12,080) nm; MS (LIFDI): *m/z* (%) 593.2 (100); analysis (calculated, found for C₂₁H₄₀N₃O₂Pt): C (42.49, 42.86%), H (6.79, 6.87%), N (4.72, 4.72%).

[PtNPM₃(PNP)] (5). Complex **1** (8.2 mg, 0.014 mmol, 1.00 equiv.) was dissolved in a solution of C₆D₆ (0.4 ml) and PMe₃ (1 M in toluene, 80 μL, 5.79 equiv.). The mixture was photolysed (λ_{exc} > 305 nm) at room temperature for 1 h. ¹H{³¹P} NMR spectroscopic monitoring indicated the formation of phosphoraneiminato product **5** in around 75% yield. Isolation required repeated recrystallization from Et₂O at -36 °C, leading to low yields (<10%) of spectroscopically clean, light yellow crystals of **5** that were suitable for characterization by X-ray diffraction: ¹H NMR (400.25 MHz, C₆D₆, 298 K): δ (ppm) 6.93 (A₁₈XX'A'₁₈, N = |³J_{HP} + ⁴J_{HP}| = 38.0 Hz, ³J_{HH} = 5.2 Hz, ³J_{PH} = 63.2 Hz, 2H, NCH), 4.08 (A₁₈XX'A'₁₈, N = |³J_{HP} + ⁴J_{HP}| = 8.8 Hz, ³J_{HH} = 4.8 Hz, ³J_{PH} = 33.6 Hz, 2H, PCH), 1.45 (A₁₈XX'A'₁₈, N = |³J_{HP} + ⁵J_{HP}| = 14.0 Hz, 36H, CMe₃), 1.42 (s, PMe₃, slightly overlapped with the signal of CMe₃); ¹³C{¹H} NMR (100.65 MHz, C₆D₆, 298 K): δ (ppm) 162.4 (t, ²J_{PC} = 7.5 Hz, NCH), 83.0 (t, ¹J_{PC} = 22.4 Hz, CHP), 35.6 (t, ¹J_{PC} = 11.9 Hz, PCMe₃), 29.7 (t, ²J_{PC} = 3.1 Hz, PCMe₃), 24.0 (d, ¹J_{PC} = 63.1 Hz, PMe₃); ³¹P{¹H} NMR (121.5 MHz, C₆D₆, 298 K): δ (ppm) 56.9 (s, ¹J_{PP} = 2,882 Hz, PCMe₃), -29.5 (s, ¹J_{PP} = 675 Hz, NPM₃); MS (LIFDI): *m/z* (%) 641.1 (100).

[PtNH(C(O)Ph)(PNP)] (6). Complex **1** (8.0 mg, 0.013 mmol, 1.00 equiv.) and PhCHO (1.5 μL, 0.015 mmol, 1.1 equiv.) were dissolved in toluene-d₈ (0.4 ml). The solution was photolysed (λ_{exc} > 305 nm) at -30 °C for 2.5 h. After removal

of solvent and washing with cold pentane, complex **6** (yield 7.5 mg, 83%) was obtained. Crystals suitable for X-ray diffraction were obtained by crystallization from a saturated solution in pentane at -36 °C: ¹H NMR (400.25 MHz, C₆D₆, 298 K): δ (ppm) 8.14–8.08 (m, 2H, C(=O)Ph), 7.26–7.20 (m, 2H, C(=O)Ph), 7.15–7.10 (m, 1H, C(=O)Ph), 6.73 (A₁₈XX'A'₁₈, N = |³J_{HP} + ⁴J_{HP}| = 37.6 Hz, ³J_{HH} = 5.6 Hz, ³J_{PH} = 65.6 Hz, 2H, NCH), 4.55 (broad, ²J_{PH} = 23.2 Hz, 1H, NH), 4.00 (A₁₈XX'A'₁₈, N = |³J_{HP} + ⁴J_{HP}| = 8.8 Hz, ³J_{HH} = 5.2 Hz, ³J_{PH} = 32.8 Hz, 2H, PCH), 1.35 (A₁₈XX'A'₁₈, N = |³J_{HP} + ⁵J_{HP}| = 14.0 Hz, 36H, CMe₃); ¹³C{¹H} NMR (100.65 MHz, C₆D₆, 298 K): δ (ppm) 170.8 (s, C(=O)Ph), 162.5 (t, ²J_{PC} = 7.3 Hz, NCH), 141.5 (s, C(=O)Ph), 128.9 (s, C(=O)Ph), 127.2 (s, C(=O)Ph), 83.3 (t, ¹J_{PC} = 22.8 Hz, CHP), 36.4 (t, ¹J_{PC} = 12.8 Hz, PCMe₃), 29.2 (t, ²J_{PC} = 3.1 Hz, PCMe₃); ³¹P{¹H} NMR (162.02 MHz, C₆D₆, 298 K): δ (ppm) 61.9 (s, ¹J_{PP} = 2,720.5 Hz); ¹⁹⁵Pt{¹H} NMR (107.14 MHz, C₆D₆, 298 K): δ (ppm) -3,905.8 (t, ¹J_{PP} = 2,744.9 Hz); IR (ATR): 3,410 (N-H), 1,613 (C=O), 1,528 (C=C) cm⁻¹; UV-vis (THF): λ_{max} (ε, M⁻¹ cm⁻¹) = 247 (13,160), 288 (14,650), 318 (16,560) nm; MS (LIFDI): *m/z* (%) 671.3 (100); analysis (calculated, found for C₂₇H₄₆N₂O₂Pt): C (48.28, 48.17%), H (6.90, 7.00%), N (4.17, 4.28%).

[PtNH(C(O)(*n*-C₃H₇))(PNP)] (7). Complex **1** (7.6 mg, 0.013 mmol, 1.00 equiv.) and *n*-C₃H₇CHO (1.7 μL, 0.019 mmol, 1.5 equiv.) were dissolved in toluene-d₈ (0.4 ml). The solution was photolysed (λ_{exc} > 305 nm) at -30 °C for 2.5 h. Removal of the solvent gave complex **7** (yield 7 mg, 86%). Crystals suitable for X-ray diffraction were obtained by crystallization from a saturated solution in pentane at -36 °C: ¹H NMR (400.25 MHz, C₆D₆, 298 K): δ (ppm) 6.72 (A₁₈XX'A'₁₈, N = |³J_{HP} + ⁴J_{HP}| = 37.2 Hz, ³J_{HH} = 5.2 Hz, ³J_{PH} = 65.6 Hz, 2H, NCH), 4.00 (A₁₈XX'A'₁₈, N = |³J_{HP} + ⁴J_{HP}| = 8.8 Hz, ³J_{HH} = 5.2 Hz, ³J_{PH} = 32.8 Hz, 2H, PCH), 3.33 (broad, ²J_{PH} = 27.6 Hz, 1H, NH), 2.26 (t, ³J_{HH} = 7.5 Hz, 2H, COCH₂), 1.91 (sext, ³J_{HH} = 7.5 Hz, 2H, COCH₂CH₂), 1.36 (A₁₈XX'A'₁₈, N = |³J_{HP} + ⁵J_{HP}| = 14.4 Hz, 36H, CMe₃), 1.04 (t, ³J_{HH} = 7.5 Hz, 3H, CH₂CH₃); ¹³C{¹H} NMR (100.65 MHz, C₆D₆, 298 K): δ (ppm) 175.4 (s, CO), 162.5 (t, ²J_{PC} = 7.4 Hz, NCH), 83.3 (t, ¹J_{PC} = 22.7 Hz, CHP), 42.7 (s, COCH₂), 36.4 (t, ¹J_{PC} = 12.6 Hz, ²J_{PC} = 33.2 Hz, PCMe₃), 29.2 (t, ²J_{PC} = 3.0 Hz, PCMe₃), 20.7 (s, COCH₂CH₂), 14.9 (s, CH₂CH₃); ³¹P{¹H} NMR (162.02 MHz, C₆D₆, 298 K): δ (ppm) 61.2 (s, ¹J_{PP} = 2,740.9 Hz); ¹⁹⁵Pt{¹H} NMR (107.14 MHz, C₆D₆, 298 K): δ (ppm) -3,895.5 (t, ¹J_{PP} = 2,759.9 Hz); IR (ATR): 3,381 (N-H), 1,608 (C=O), 1,528 (C=C) cm⁻¹; UV-Vis (THF): λ_{max} (ε, M⁻¹ cm⁻¹) = 247 (7,870), 291 (10,400), 320 (15,070) nm; MS (LIFDI): *m/z* (%) 637.2 (100); analysis (calculated, found for C₂₄H₄₆N₂O₂Pt): C (45.20, 45.48%), H (7.59, 7.38%), N (4.39, 4.30%).

[PtNH(Bpin)(PNP)] (8). Complex **1** (8.6 mg, 0.014 mmol, 1.00 equiv.) and HBpin (3 μL, 0.021 mmol, 1.5 equiv.) were dissolved in C₆D₆ (0.4 ml). The solution was photolysed (λ_{exc} > 305 nm) at room temperature for 1.5 h. Removal of the solvent gave complex **8** (yield 8.5 mg, 85%). Crystals suitable for X-ray diffraction were obtained by crystallization from a saturated solution in pentane at -36 °C: ¹H NMR (300.15 MHz, C₆D₆, 298 K): δ (ppm) 6.81 (A₁₈XX'A'₁₈, N = |³J_{HP} + ⁴J_{HP}| = 36.8 Hz, ³J_{HH} = 5.5 Hz, ³J_{PH} = 60.0 Hz, 2H, NCH), 4.02 (A₁₈XX'A'₁₈, N = |³J_{HP} + ⁴J_{HP}| = 8.6 Hz, ³J_{HH} = 5.3 Hz, ³J_{PH} = 33.3 Hz, 2H, PCH), 1.39 (A₁₈XX'A'₁₈, N = |³J_{HP} + ⁵J_{HP}| = 13.9 Hz, 36H, CMe₃), 1.30 (s, 12H, OC(CH₃)₂), -0.06 (broad, ²J_{PH} = 19.5 Hz, 1H, NH); ¹³C{¹H} NMR (100.65 MHz, C₆D₆, 298 K): δ (ppm) 162.6 (t, ²J_{PC} = 7.4 Hz, NCH), 83.3 (t, ¹J_{PC} = 22.3 Hz, CHP), 36.2 (t, ¹J_{PC} = 12.6 Hz, PCMe₃), 29.6 (t, ²J_{PC} = 3.0 Hz, ²J_{PC} = 14.2 Hz, PCMe₃), 25.8 (s, OC(CH₃)₂); ³¹P{¹H} NMR (162.02 MHz, C₆D₆, 298 K): δ (ppm) 55.8 (s, ¹J_{PP} = 2,783.0 Hz); ¹⁹⁵Pt{¹H} NMR (107.17 MHz, C₆D₆, 298 K): δ (ppm) -3,789.2 (t, ¹J_{PP} = 2,798.5 Hz); IR (ATR): 3,277 (N-H), 1,526 (C=C) cm⁻¹; UV-vis (THF): λ_{max} (ε, M⁻¹ cm⁻¹) = 246 (7,830), 306 (13,270), 320 (12,860) nm; MS (LIFDI): *m/z* (%) 693.3 (100); analysis (calculated, found for C₂₆H₃₃BN₂O₂Pt): C (45.03, 45.14%), H (7.70, 7.40%), N (4.04, 4.14%).

[PtNPh(BPh₂)(PNP)] (9). Complex **1** (12.5 mg, 0.021 mmol, 1.00 equiv.) and BPh₃ (5.8 mg, 0.024 mmol, 1.14 equiv.) were dissolved in toluene-d₈ (0.4 ml). The solution was photolysed (λ_{exc} > 305 nm) at -30 °C for 2.5 h. After removal of the solvent, extraction with Et₂O/pentane and filtration, crystalline **9** (yield 6.6 mg, 39%) was obtained after two crystallizations at -36 °C. Crystals suitable for X-ray diffraction were obtained by crystallization from a saturated solution in pentane at -36 °C: ¹H NMR (400.25 MHz, C₆D₆, 298 K): δ (ppm) 8.93 (d, ³J_{HH} = 6.5 Hz, 2H, NPh), 7.53 (d, ³J_{HH} = 8.1 Hz, 2H, BPh₂), 7.44 (d, ³J_{HH} = 7.2 Hz, 2H, BPh₂), 7.32–7.21 (m, 3H, NPh), 7.21–7.17 (m, 2H, BPh₂), 7.09 (t, ³J_{HH} = 7.5 Hz, 1H, BPh₂), 6.96 (t, ³J_{HH} = 7.7 Hz, 2H, BPh₂), 6.75 (t, ³J_{HH} = 7.2 Hz, 1H, BPh₂), 6.47 (A₁₈XX'A'₁₈, N = |³J_{HP} + ⁴J_{HP}| = 36.4 Hz, ³J_{HH} = 6.0 Hz, ³J_{PH} = 56.8 Hz, 2H, NCH), 3.83 (A₁₈XX'A'₁₈, N = |³J_{HP} + ⁴J_{HP}| = 8.1 Hz, ³J_{HH} = 5.3 Hz, ³J_{PH} = 30.7 Hz, 2H, PCH), 1.23–1.11 (m, 36H, CMe₃); ¹³C{¹H} NMR (100.65 MHz, C₆D₆, 298 K): δ (ppm) 161.8 (t, ²J_{PC} = 6.7 Hz, NCH), 160.4 (s, NPh), 139.2 (s, NPh), 135.7 (s, BPh₂), 131.2 (s, BPh₂), 129.1 (s, NPh), 127.0 (s, BPh₂), 126.73 (s, BPh₂), 126.66 (s, NPh), 126.0 (s, BPh₂), 121.2 (s, BPh₂), 84.3 (t, ¹J_{PC} = 22.7 Hz, CHP), 38.5 (t, ¹J_{PC} = 11.9 Hz, PCMe₃), 36.2 (t, ¹J_{PC} = 11.4 Hz, PCMe₃), 29.6 (t, ²J_{PC} = 2.3 Hz, PCMe₃), 29.5 (t, ²J_{PC} = 2.3 Hz, PCMe₃); ³¹P{¹H} NMR (162.02 MHz, C₆D₆, 298 K): δ (ppm) 51.4 (s, ¹J_{PP} = 2,961.5 Hz); ¹⁹⁵Pt{¹H} NMR (107.17 MHz, C₆D₆, 298 K): δ (ppm) -3,466.5 (t, ¹J_{PP} = 2,986.8 Hz); IR (ATR): 1547 (C=C) cm⁻¹; UV-vis (THF): λ_{max} (ε, M⁻¹ cm⁻¹) = 230 (31,640), 249 (24,300), 310 (27,510) nm; MS (LIFDI): *m/z* (%) 807.4 (100); analysis (calculated, found for C₃₈H₃₃BN₂P₂Pt): C (56.51, 56.39%), H (6.86, 6.81%), N (3.47, 3.45%).

Data availability

All data generated and analysed during this study are included in this Article and its Supplementary Information or are available from the corresponding author upon reasonable request. Crystallographic data for the structures reported in this article have been deposited at the Cambridge Crystallographic Data Centre, under deposition numbers CCDC 1973273 ([PtCl(N(CH₂CH₂P^tBu₂)₂)] (A)), 1973274 ([PtCl(PNP)] (B)), 1973275 ([PtH(PNP)] (C)), 1973276 ([PtOTf(PNP)] (D)), 1973277 (1), 1973278 (2), 1973279 (3), 1994705 (5), 1973280 (6), 1973281 (7), 1973282 (8), 1973283 (9). Copies of the data can be obtained free of charge via <https://www.ccdc.cam.ac.uk/structures/>.

Acknowledgements

The authors thank the ERC (Grant Agreement 646747) and the German Research Council (DFG grants 389479699/RTG2455, SCHN950/6-1 and SL104/10) for funding. J. M. Matys is acknowledged for help with synthetic work and single-crystal growth of (Pt(OTf)(PNP)). C.W. thanks R. Herbst-Irmer for helpful discussions. Quantum chemical calculations of the Frankfurt group were performed at the Center for Scientific Computing (CSC) Frankfurt on the Goethe-HLR computer cluster.

Author contributions

S.S. and M.C.H. generated the project and designed its concept. S.S. supervised the experimental study and M.C.H. the quantum chemical study. J.S. performed synthetic and spectroscopic work. J.A. carried out spectroscopic and crystallographic work. C.W. performed crystallographic characterization. B.d.B., M.D. and H.V. carried out quantum chemical calculations. D.H. carried out the magnetic characterization supervised by J.v.S. All authors discussed the results in detail and commented on the manuscript.

Competing interests

The authors declare no competing interests.

Additional information

Supplementary information is available for this paper at <https://doi.org/10.1038/s41557-020-0522-4>.

Correspondence and requests for materials should be addressed to M.C.H. or S.S.

Reprints and permissions information is available at www.nature.com/reprints.